

Experimental and Numerical Study on Shock Layer Radiation for Planetary Entry Flights

Gouji Yamada, Shota Ago, Yuto Kubo, Takashi Matsuno, Hiromitsu Kawazoe
 Department of Mechanical and Aerospace Engineering, Tottori University
 4-101 Koyama-Minami, Tottori, 680-8552, Japan
 E-mail: yamada@mech.tottori-u.ac.jp

Abstract

In this study, shock layer radiation is investigated by experimental and numerical approach. Radiation profiles of N_2 , N_2^+ , and N are observed in two test conditions of initial pressure and velocity by time-resolved emission spectroscopy. Flow properties behind shock front are computed by the CFD code with two-temperature thermochemical model. The results are used as inputs for the radiation analysis code "SPRADIAN 2" to derive the radiation profiles behind shock front along the line of sight. Comparison between experiments and calculations shows that the decline of calculated radiation intensity is slower than that of measured one. Therefore, the present calculation fails to reproduce the measured radiation profile. This is considered to be due to the fact that the two-temperature model seems to lose its accuracy in the intermediate hypersonic flow regime. Further investigations are necessary to improve the accuracy of the two-temperature model.

Key words: shock tube, shock layer radiation, thermochemical nonequilibrium, spectroscopy, planetary entry

Nomenclature

C	: reaction rate constant, $m^3/(mol \cdot s)$
k_f	: forward reaction rate coefficient, $cm^3 \text{ mole}^{-1} s^{-1}$
M	: unspecified third body
n	: temperature exponent on reaction-rate coefficient
P_0	: ambient pressure ahead of the shock wave, Pa
T_a	: geometric average temperature, $\sqrt{TT_v}$, K
T_d	: characteristic temperature, K
T_t	: translational - rotational temperature, K
T_v	: vibrational - electron - electronic excitation temperature, K
T_x	: unspecified temperature (T_t , T_a , or T_v), K
t	: time from shock front, μs
V	: shock velocity, km/s
X	: distance from shock front, mm

Introduction

Thermochemical nonequilibrium process in the shock layer around hypersonic vehicles is important for the development of the vehicles because it plays an important role in determining aerodynamic characteristics and heating rates of the vehicles. Assessments of entry flight environments have been conducted by the numerical simulation based on computational fluid dynamics (CFD) with thermochemical model. The result relies on the accuracy of the model applied in the simulation. In past studies, some thermochemical models were developed and applied for the assessments of flight environments [1-4]. However, the accuracy of these models is limited due to the lack of experimental data. To improve the model accuracy, the validation of the models is necessary by experimental investigations. One of the authors conducted shock-tube experiments to validate the two-temperature kinetic model developed by Park [5-6]. In these studies, the spatial distribution of emission spectra was measured by the time-frozen spectroscopy. The temperatures of chemical species in the shock layer are

deduced from the measured spectra and compared with the temperatures calculated by the two-temperature model. The results showed the measured temperatures disagreed with the calculated temperatures immediately behind shock waves. In these studies, validations were conducted in terms of the temperatures and the discrepancy of the model assumption was made clear. Chemical processes in the shock layer are important to assess the entry flight environments. However, the accuracy of the reaction rate coefficients used in the thermochemical model is questionable because the reaction rate coefficients were deduced from the comparison with limited experimental data. Temporal profiles of shock layer radiation depend on the chemical process in the shock layer. Therefore, investigations of shock layer radiation are useful to validate the reaction rate coefficients.

The purpose of the present study is to investigate shock layer radiation by experimental and numerical approach. In this study, time-resolved radiation measurements are conducted using the hypersonic shock tube at the Tottori University. Temporal radiation profiles of N_2 , N_2^+ , and N are measured in two different conditions of initial pressure and velocity. Flow properties behind shock front are calculated by the CFD code with the two-temperature model. The flow properties are used as inputs for radiation analysis code "SPRADIAN 2" and the calculated radiation profiles is obtained by radiation calculations. Comparisons between experiments and calculations are conducted to validate the reaction rate coefficient used in the CFD code.

Shock-Tube Measurement

A. Shock-tube facility

Experimental investigations have been carried out using the hypersonic shock tube developed at the Tottori University. A schematic drawing of the shock tube is shown in Fig.1. The shock tube is composed of a high pressure reservoir, a compression tube, a low pressure tube, vacuum tank, and a free piston driving in the compression tube. The shock-tube facility is located on movable mounts and connected to the vacuum tank by the shock absorbing mechanism to protect the facility from the impact produced by the piston operations. This facility works according to the Stalker principle. The free piston driven by high-pressure nitrogen adiabatically compresses the helium used as a driver gas. When the pressure in the helium reaches a critical value, a steel diaphragm bursts and a shock wave is formed in the low pressure tube where the test gas is filled. The low pressure tube with 44 mm square cross-section is made of aluminum alloy to reduce emissions from impurities. The test section with four quartz windows are located 2300 mm downstream from the diaphragm. The compression tube and low pressure tubes are evacuated to the pressure of 5.0 Pa using oil rotary and root pumps before the filling of a test gas. The facility can generate shock velocities ranging from 4.0 to 7.0 km/s with test gases of air, N_2 , CO_2 , and $CO_2 - N_2$ mixture, covering the planetary entry flight conditions.

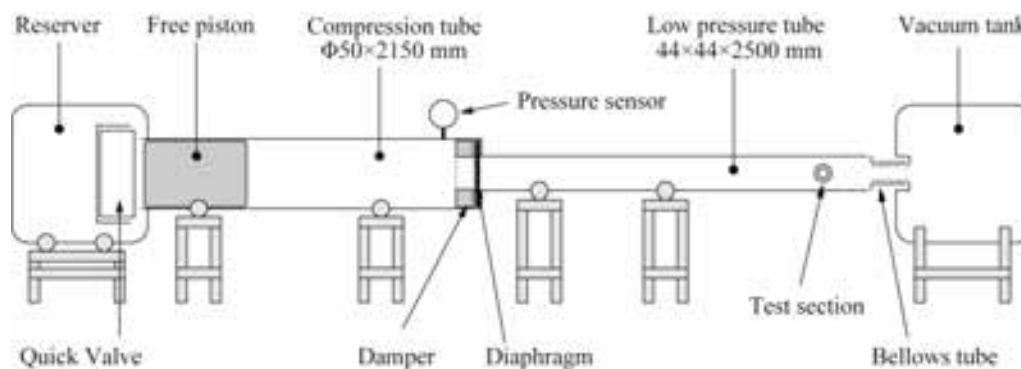


Fig.1 A schematic drawing of the hypersonic shock tube

B. Optical instrumentation

A schematic drawing of the optical instrumentation at the test section is shown in Fig.2. The shock velocity at the test section is measured by the double-laser schlieren measurement system [7]. Two laser beams are aligned along the flow direction in line to pass through the test section perpendicularly to the axis of the shock-tube flow. The optical path is adjusted by flat mirrors to reach separate avalanche photodiodes (APD). Deflection of the beams as a result of a density gradient at the shock front causes a change in the output signals of avalanche photodiodes. The shock velocity at the test section can be obtained from the beam distance and the time difference of the output signals.

Time-resolved emission spectroscopy is conducted to measure the radiation emitted from the shock layer. This technique provides information on the evolution of the radiation as a function of time. A monochromator (JASCO, CT-25C) is used with a 1200 g/mm grating and the entrance slit is fixed at 50 μ m. A quartz convex lens is used to focus the radiation on the entrance slit of the monochromator. To record the radiation, a photomultiplier tube (PMT) (Hamamatsu, R928) is placed behind the exit slit of the monochromator. The spectral response of the PMT ranges from 185 to 900 nm and its peak sensitivity is at 400 nm. The rise time of the PMT is 2.2 ns. The exit slit is variable depending on the measured wavelength range. The signal produced by the PMT is recorded by a digital oscilloscope (Agilent Technologies, DSOX2024A). An avalanche photodiode is placed on the other side of the monochromator to measure the total radiation intensity and its signal is used to trigger the oscilloscope at the instant of the shock arrival.

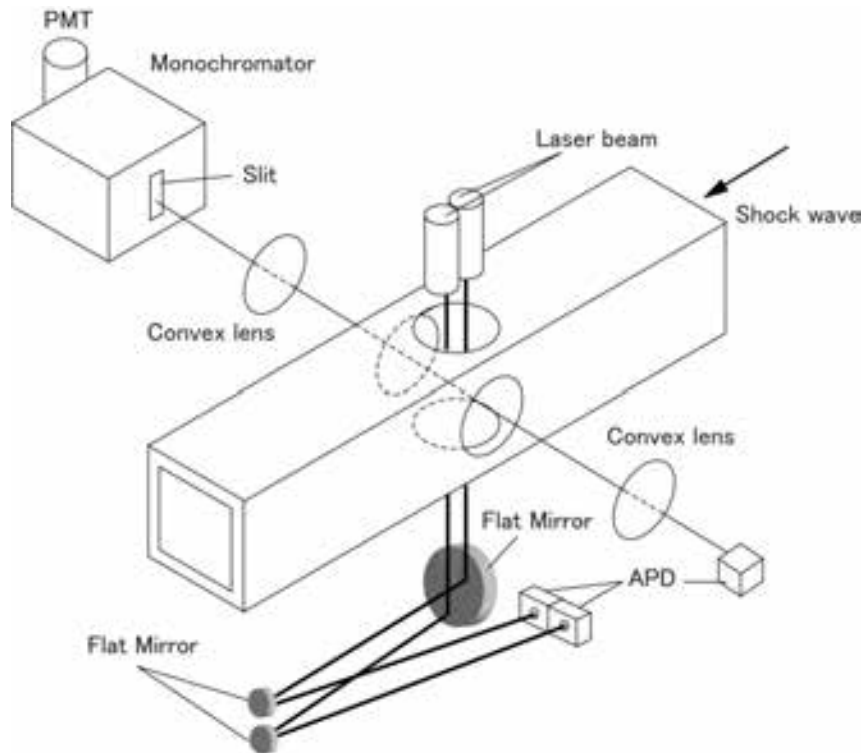


Fig.2 A schematic drawing of the optical instrumentation

C. Test conditions

Experiments are carried out using pure N₂ as a test gas simulating the Earth atmosphere. Air is not used in this study because the physical processes are more difficult than those in N₂. Test conditions are shown in Table 2. Two initial pressure /shock velocity conditions are studied: $p = 100$ Pa and $v = 5.5$ km/s (case1), $p = 500$ Pa, $v = 4.68$ km/s (case2). For these conditions, N₂ (2+) (1,0) band head, N₂⁺ (1-) (0, 0) band head, and N 3p 4S⁰ - 3s⁴P triplet are monitored using the monochromator configurations listed in Table 3.

Table 1 Test conditions

Case	Pressure, Pa	Shock velocity, km/s	Test gas
1	100	5.50	N ₂
2	500	4.68	N ₂

Table 2 Monochromator configurations

Configuration	Grating density, g/mm	Center wavelength, nm	Wavelength span, nm	Features targeted
1	1200	316	2	N ₂ (2+) (1,0)
2	1200	391	4	N ₂ ⁺ (1-) (0,0)
3	1200	744	6	N 3p 4S ⁰ - 3s ⁴ P

Numerical Simulation

Numerical simulations are carried out to reproduce the measured temporal profile of the shock layer radiation. The flow properties in the shock layer are obtained using the CFD code which solves the one-dimensional Navier-Stokes equations with thermochemical model. The two-temperature model developed by Park is employed for the thermochemical nonequilibrium in the code. Chemical species considered are N_2 , N , N_2^+ , N^+ , and e^- . Following Park [8], a set of six reactions related to nitrogen is taken into account. The reactions and the corresponding rate coefficients are shown in Table 3. In the present calculation, a shock wave is generated by impinging a hypersonic flow to a wall instead of solving the shock tube problem. This method is suitable to investigate the thermochemical nonequilibrium phenomena behind the shock front because the effect of expansion waves can be reduced. Figure 3 shows the computational region used for the calculation: 300 grid points corresponding to a grid spacing of 167 μm . After the hypersonic flow impinges the wall, a shock wave is generated and then the computation starts. The generated shock wave propagates leftward and calculations are conducted until the shock wave arrives at 5mm. The governing equations are integrated by a cell-centered finite volume scheme. The inviscid fluxes are evaluated by the AUSM-DV scheme [9] whose spatial accuracy is extended to second-order using the MUSCL approach [10] with the minmod limiter. The viscous fluxes are evaluated by central differencing. Time integration is performed with a CFL number of 0.1, which is combined with the diagonal point implicit method [11] for maintaining the stability of the source term.

The flow properties (temperatures and densities) calculated by the CFD code are used as input parameters for the radiation analysis code SPRADIAN 2 [12] to derive temporal profiles of the radiation along the line of sight. In the SPRADIAN2, the spectral emission and absorption coefficients are obtained at the given thermochemical conditions using a line-by-line technique. The radiation intensity is obtained by integrating the radiative transfer equation across the test section of the shock tube. The resulting intensity values are integrated over the wavelength intervals corresponding to the observation.

Table 3 Chemical reactions and the reaction rate coefficient

Reactions	M	C	n	T_d	T_x	Source
Dissociation reaction						
1	$N_2 + M \rightarrow 2N + M$	N_2, N_2^+	7.0^{15}	-1.60	113200	T_a Ref.[4]
2	$N_2 + M \rightarrow 2N + M$	N, N^+	3.0^{16}	-1.60	113200	T_a Ref.[4]
3	$N_2 + e^- \rightarrow 2N + e^-$		3.0^{18}	-1.60	113200	T_v Ref.[18]
Associative ionization						
4	$N + N \rightarrow N_2^+ + e^-$		4.4^1	1.50	67500	T_t Ref.[4]
Electron impact ionization						
5	$N + e^- \rightarrow N^+ + e^-$		2.5^{28}	-3.82	168600	T_v Ref.[4]
Charge exchange reaction						
6	$N_2 + N^+ \rightarrow N_2^+ + N$		1.0^6	0.50	12200	T_t Ref.[4]

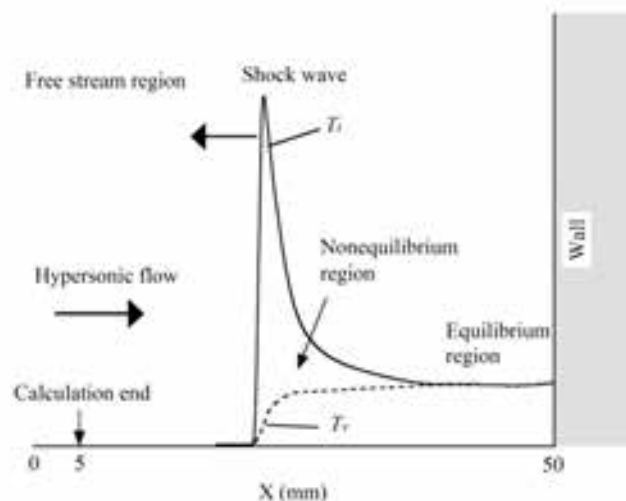


Fig.3 Computational region

Results and Discussion

Figure 4 shows the calculated flow properties for the case 1. The vibrational-electron-electronic temperature, T_v is significantly lower than the translational-rotational temperature, T_t immediately behind shock front. In this region, T_v is raised through the collisional processes. The equilibration between T_t and T_v are accomplished in the region after 20 μ s. Dissociation of N_2 is significant and the molar fraction of N almost reaches 0.2, but ionization is fairly weak at the calculated condition. Figure 5 shows the calculated radiation spectrum using the flow properties in Fig. 4. The radiation intensity in the ultraviolet (UV) region is higher than that in visible (VIS) and near infrared light (NIR) regions. The spectrum in UV region is dominated by $N_2(2+)$ and $N_2^+(1-)$ band systems. The spectrum in VIS and NIR regions are dominated by $N_2(1+)$ band system and atomic line of N. Figure 6 shows the detail spectra in the UV and VIS regions, respectively. In the UV region, many band head of $N_2(2+)$ and $N_2^+(1+)$ can be identified. Band heads of $N_2(2+)(1,0)$ at 315.9 nm and $N_2^+(0,0)$ at 391 nm are measured in this study because the band heads are unobstructed and are free from other band systems. In the VIS region, there are many band heads of $N_2(1+)$. However, their band heads are not clear. Atomic lines of N $3p\ 4S^0 - 3s\ 4P$ triplet are seen at around 750 nm. The atomic spectrum of N is measured in this study.

The measured temporal profiles of radiation intensity are shown in Figs 7, and 8 for two cases. In these figures, the calculated temporal profiles of radiation intensity are shown as dashed lines. The measured and calculated radiation intensities are normalized by the maximum value for comparison. The rapid increase of the radiation is seen immediately behind shock front. The rapid increase of the radiation is called radiation overshoot [13]. This is caused by the nonequilibrium radiation from the excited species. After the peak, the radiation intensity decreases slowly and plateaus. The measured radiation profiles are different from the calculated radiation profiles in all figures. Especially, the decline of the measured radiation intensity is much slower than the calculated one. This difference is considered to be caused by the boundary-layer growth on the inner wall of the shock tube [14]. In the boundary layer, the test gas is adiabatically compressed and the temperature and densities are increased, resulting in the rise in radiation intensity. Therefore, the decline of the measured radiation intensity becomes slower than the calculated one. Disagreement becomes more significant in case 2, where shock velocity is slower than that in case 1. The two-temperature model was validated and its accuracy was demonstrated in flight conditions at around 6 km/s [8, 15]. Past studies showed that the two-temperature model failed to reproduce the measured shock standoff distances in the intermediate hypersonic flow regime from 2.5 to 4.5 km/s [16, 17]. In this flow regime, the two-temperature model seems to lose its accuracy. In the present study, the two-temperature model is validated by radiation measurements in the conditions closer to the intermediate hypersonic flow regime. Therefore, the present calculation fails to reproduce the measured radiation profiles. Further investigations are necessary to improve the accuracy of the two-temperature model in the intermediate hypersonic flow regime.

Conclusion

Shock layer radiation is investigated by shock tube measurements and CFD simulations coupled with radiation calculations. The temporal radiation profiles of N_2 , N_2^+ and N are measured by the time-resolved spectroscopy and compared with the numerical calculations. The measured radiation profiles disagree with the calculated one. Disagreement is more significant in case 2, where shock velocity is slower than that in case 1. The present calculation fails to reproduce the measured radiation profile. This is because that the two-temperature model seems to lose its accuracy in the present test conditions. Modification of the model is necessary by further investigations.

Acknowledgment

This work was supported by the Grant-in-Aid for young Scientists (B) (No. 23760770), provided by the Japan Society for the Promotion of Science.

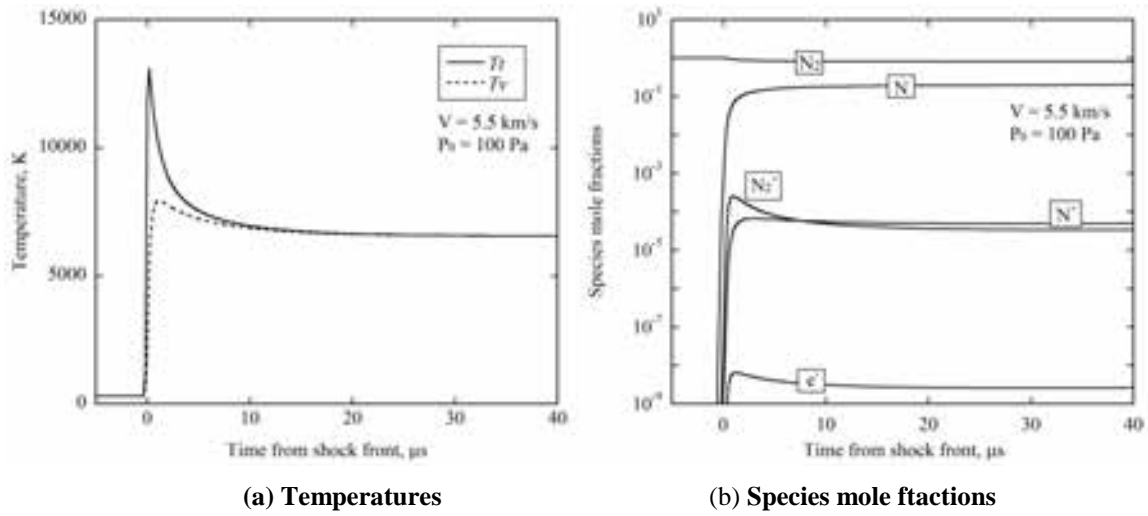


Fig.4 calculated flow properties behind shock front for case1

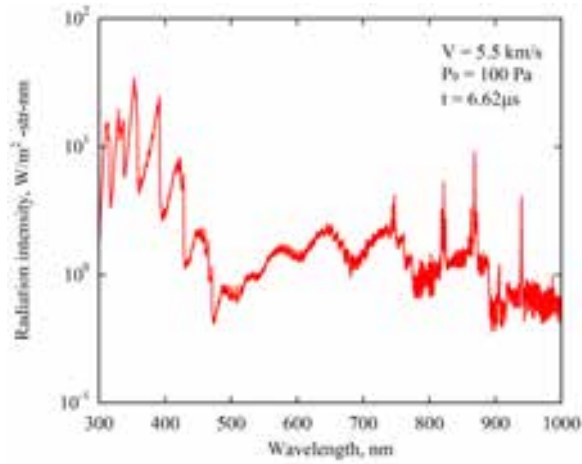


Fig.5 Calculated emission spectrum for case1

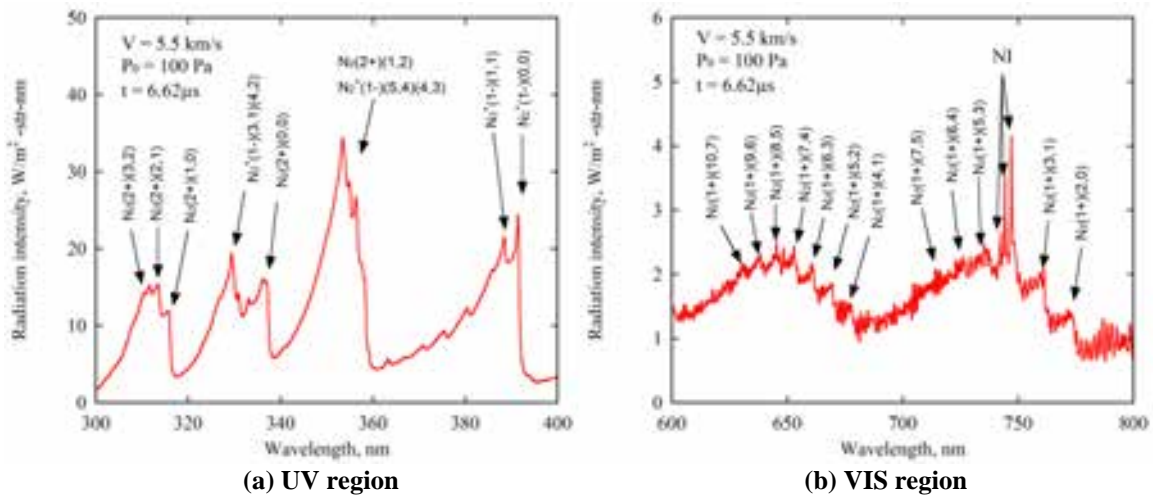
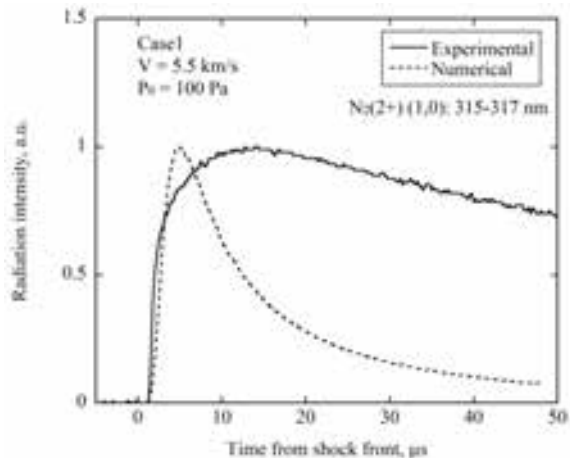
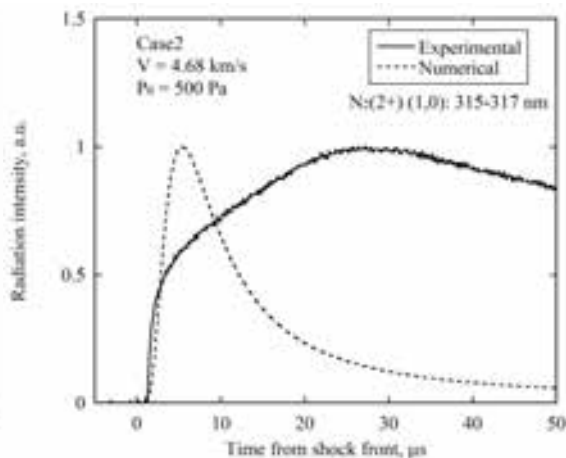


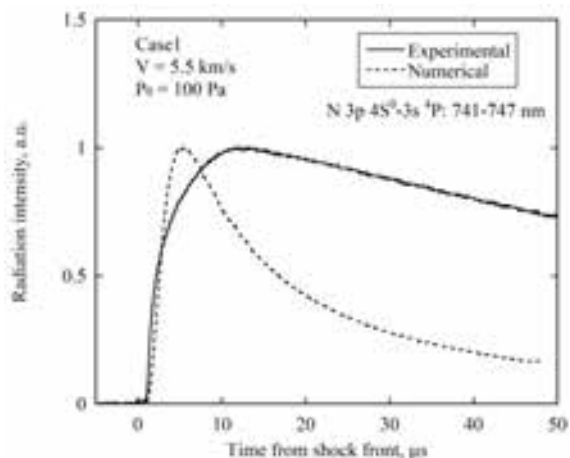
Fig.6 Calculated UV and VIS spectra for case 1



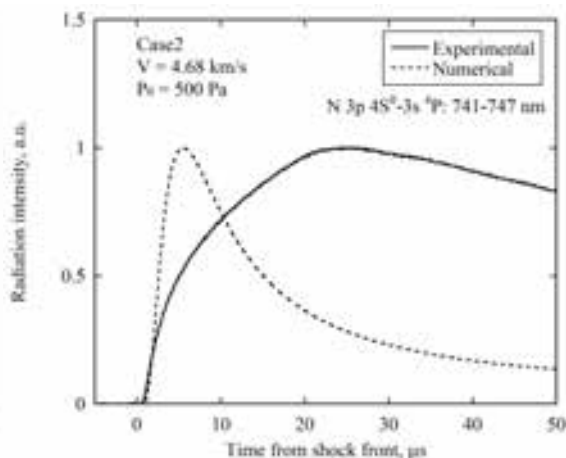
a) $N_2(2+)(1,0)$



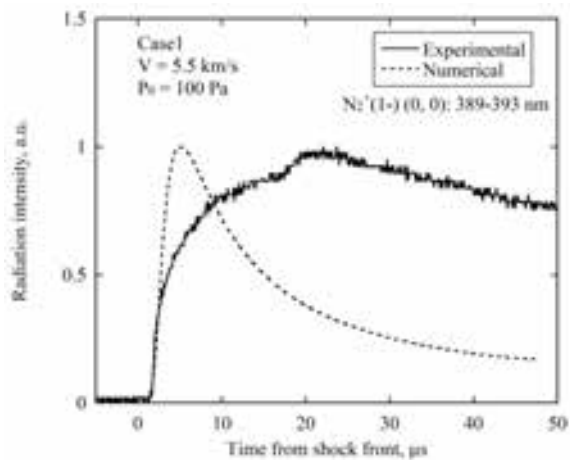
a) $N_2(2+)(1,0)$



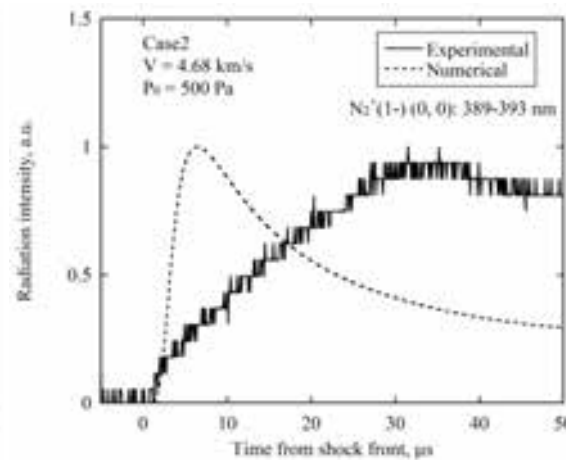
b) $N 3p 4S^0 - 3s ^4P$



b) $N 3p 4S^0 - 3s ^4P$



c) $N_2^+(1-)(0,0)$



c) $N_2^+(1-)(0,0)$

Fig.7 Comparison result for case1

Fig.8 Comparison result for case2

References

- [1] Park, C.: Nonequilibrium Hypersonic Aerothermodynamics, John Wiley & Sons, New York, 1990.
- [2] Gnoffo, P. A., Gupta, R. N., and Shinn, J. L.: Conservation Equations and Physical Models for Hypersonic Air Flows in Thermal and Chemical Nonequilibrium, *NASA TP-2867*, 1989.
- [3] Gupta, R. N., Yos, J. M., Thompson, R. A., and Lee, K. P.: A Review of Reaction rates and Thermodynamic and Transport Properties for the 11-Species Air Model for Chemical and Thermal Nonequilibrium Calculations to 30000 K, *NASA TM-101528*, 1989.
- [4] Park, C.: Review of Chemical-Kinetic Problems of Future NASA Missions, I: Earth Entries, *Journal of Thermophysics and Heat Transfer*, Vol. 7, No. 3, pp. 385-398, 1993.
- [5] Yamada, G., TAKAYANAGI, H., SUZUKI, T. and FUJITA, K.: Shock Layer Radiation Analysis using a Hypervelocity Shock Tube (HVST), *Transactions of the Japan Society for Aeronautical and Space Sciences* Vol. 55, pp.37-43, 2012.
- [6] Yamada, G., TAKAYANAGI, H., SUZUKI, T. and FUJITA, K.: Analysis of Shock Layer Radiation from the Vacuum-Ultraviolet to Near-Infrared Regions, *Transactions of the Japan Society for Aeronautical and Space Sciences* Vol. 55, pp.60-67, 2012.
- [7] Yamada, G., SUZUKI, T., TAKAYANAGI, H. and FUJITA, K.: Development of Shock Tube for Ground Testing Reentry Aerothermodynamics, *Transactions of the Japan Society for Aeronautical and Space Sciences* Vol. 54, pp.51-61, 2011.
- [8] Park, C.: Assessment of a Two-Temperature Kinetic Model for Dissociating and Weakly Ionizing Nitrogen, *Journal of Thermophysics and Heat Transfer*, Vol. 2, pp. 8-16, 1988.
- [9] Wada, Y. and Liu, M. S.: A Flux Splitting Scheme with High-resolution and Robustness for Discontinuities, *AIAA Paper* 94-0083, 1994.
- [10] Anderson, W. K., Thomad, J. L., and van Leer, B.: Computation of Finite Volume Flux Vector Splitting for the Euler Equations, *AIAA Journal*, Vol. 24, pp. 1453-1460, 1986.
- [11] Everhardt, S. and Imlay, S.: Diagonal Implicit Scheme for Computing Flows with Finite Rate Chemistry, *Journal of Thermophysics and Heat Transfer*, Vol. 6, , pp. 208-216, 1992.
- [12] Fujita, K., Mizuno, M., Ishida, K., Ito, T., Spectroscopic Flow Evaluation in Inductively Coupled Plasma Wind Tunnel, *Journal of Thermophysics and Heat Transfer*, Vol.22, pp. 685-694, 2008.
- [13] Willson, J.: Ionization Rate of Air behind High-Speed Shock Waves, *The physics of Fluids*, Vol. 9, No. 10, 1966.
- [14] Park, C.: Assessment of a Two-Temperature Kinetic Model for Ionizing Air, *Journal of Thermophysics and Heat Transfer*, Vol. 3, pp. 233-244, 1989.
- [15] Sharma, P. S, and Gillespie, W.: Nonequilibrium and Equilibrium Shock Front Radiation Measurements, *Journal of Thermophysics and Heat Transfer*, Vol. 5, pp. 257-265, 1991.
- [16] Furudate M., Nonaka, S., and Sawada, K.: Behavior of Two-Temperature Model in Intermediate Hypersonic Regime, *Journal of Thermophysics and Heat Transfer*, Vol. 13, pp. 424-430.

- [17] Furudate M., Nonaka, S., and Sawada, K.: Calculation of Shock Shapes over Sharp Cone in Intermediate Hypersonic Airflow, *Journal of Thermophysics and Heat Transfer*, Vol. 13, pp. 424-430.
- [18] Park, C., Jaffe, C., and Partridge, H.: Chemical-Kinetic Parameters of Hyperbolic Earth Entry, *Journal of Thermophysics and Heat Transfer*, Vol. 15, pp. 76-89, 2001.